Growing timescales and lengthscales characterizing vibrations of amorphous solids

Ludovic Berthier[a], Patrick Charbonneau[b,c], Yuliang Jin[b,d,e,1], Giorgio Parisi[d,1], Beatriz Seoane[e,f,1], and Francesco Zamponi[e]

[a]Laboratoire Charles Coulomb, UMR 5221, Université de Montpellier and CNRS, 34095 Montpellier, France; [b]Department of Chemistry, Duke University, Durham, NC 27708; [c]Department of Physics, Duke University, Durham, NC 27708; [d]Dipartimento di Fisica, Sapienza Universitá di Roma, Istituto Nazionale di Fisica Nucleare, Sezione di Roma I, Istituto per i Processi Chimico-Fisici–Consiglio Nazionale delle Ricerche, I-00185 Rome, Italy; [e]Laboratoire de Physique Théorique, École Normale Supérieure & Université de Recherche Paris Sciences et Lettres, Pierre et Marie Curie & Sorbonne Universités, UMR 8549 CNRS, 75005 Paris, France, and [f]Instituto de Biocomputación y Física de Sistemas Complejos, 50009 Zaragoza, Spain

Contributed by Giorgio Parisi, May 23, 2016 (sent for review February 2, 2016; reviewed by Kunimasa Miyazaki and Grzegorz Szamel)

Low-temperature properties of crystalline solids can be understood using harmonic perturbations around a perfect lattice, as in Debye's theory. Low-temperature properties of amorphous solids, however, strongly depart from such descriptions, displaying enhanced transport, activated slow dynamics across energy barriers, excess vibrational modes with respect to Debye's theory (i.e., a boson peak), and complex irreversible responses to small mechanical deformations. These experimental observations indirectly suggest that the dynamics of amorphous solids becomes anomalous at low temperatures. Here, we present direct numerical evidence that vibrations change nature at a well-defined location deep inside the glass phase of a simple glass former. We provide a real-space description of this transition and of the rapidly growing time- and lengthscales that accompany it. Our results provide the seed for a universal understanding of low-temperature glass anomalies within the theoretical framework of the recently discovered Gardner phase transition.

glass transition | disordered solids | Gardner transition | computer simulations | hard spheres

Understanding the nature of the glass transition, which describes the gradual transformation of a viscous liquid into an amorphous solid, remains an open challenge in condensed matter physics (1, 2). As a result, the glass phase itself is not well understood either. The main challenge is to connect the localized, or "caged," dynamics that characterizes the glass transition to the low-temperature anomalies that distinguish amorphous solids from their crystalline counterparts (3–7). Recent theoretical advances, building on the random first-order transition approach (8), have led to an exact mathematical description of both the glass transition and the amorphous phases of hard spheres in the mean-field limit of infinite-dimensional space (9). A surprising outcome has been the discovery of a novel phase transition inside the amorphous phase, separating the localized states produced at the glass transition from their inherent structures. This Gardner transition (10), which marks the emergence of a fractal hierarchy of marginally stable glass states, can be viewed as a glass transition deep within a glass, at which vibrational motion dramatically slows down and becomes spatially correlated (11). Although these theoretical findings promise to explain and unify the emergence of low-temperature anomalies in amorphous solids, the gap remains wide between mean-field calculations (9, 11) and experimental work. Here, we provide direct numerical evidence that vibrational motion in a simple 3D glass-former becomes anomalous at a well-defined location inside the glass phase. In particular, we report the rapid growth of a relaxation time related to cooperative vibrations, a nontrivial change in the probability distribution function of a global order parameter, and the rapid growth of a correlation length. We also relate these findings to observed anomalies in low-temperature laboratory glasses. These results provide key support for a universal understanding of the anomalies of glassy materials, as resulting from the diverging length- and timescales associated with the criticality of the Gardner transition.

Preparation of Glass States

Experimentally, glasses are obtained by a slow thermal or compression annealing, the rate of which determines the location of the glass transition (1, 2). We find that a detailed numerical analysis of the Gardner transition requires the preparation of extremely well-relaxed glasses (corresponding to structural relaxation timescales challenging to simulate) to study vibrational motion inside the glass without interference from particle diffusion. We thus combine a very simple glass-forming model—a polydisperse mixture of hard spheres—to an efficient Monte Carlo scheme to obtain equilibrium configurations at unprecedentedly high densities, i.e., deep in the supercooled regime. The optimized swap Monte Carlo algorithm (12), which combines standard local Monte Carlo moves with attempts at exchanging pairs of particle diameters, indeed enhances thermalization by several orders of magnitude. Configurations contain either $N = 1{,}000$ or $N = 8{,}000$ (results in Figs. 1–3 are for $N = 1{,}000$; results in Fig. 4 are for $N = 8{,}000$) hard spheres with equal unit mass m and diameters independently drawn from a probability distribution $P_\sigma(\sigma) \sim \sigma^{-3}$, for $\sigma_{\min} \le \sigma \le \sigma_{\min}/0.45$. We similarly study a 2D bidisperse model glass former and report the main results in *SI Appendix*.

We mimic slow annealing in two steps (Fig. 1). First, we produce equilibrated liquid configurations at various densities φ_g using our efficient simulation scheme, concurrently

Significance

Amorphous solids constitute most of solid matter but remain poorly understood. The recent solution of the mean-field hard-sphere glass former provides, however, deep insights into their material properties. In particular, this solution predicts a Gardner transition below which the energy landscape of glasses becomes fractal and the solid is marginally stable. Here we provide, to our knowledge, the first direct evidence for the relevance of a Gardner transition in physical systems. This result thus opens the way toward a unified understanding of the low-temperature anomalies of amorphous solids.

Author contributions: L.B., P.C., Y.J., G.P., B.S., and F.Z. designed research, performed research, analyzed data, and wrote the paper.

Reviewers: K.M., Nagoya University; and G.S., Colorado State University.

The authors declare no conflict of interest.

Data deposition: Data relevant to this work have been archived and can be accessed at doi.org/10.7924/G8QN64NT.

[1]To whom correspondence may be addressed. Email: jinyuliang@gmail.com, giorgio.parisi@roma1.infn.it, or beatriz.seoane.bartolome@lpt.ens.fr.

This article contains supporting information online at www.pnas.org/lookup/suppl/doi:10.1073/pnas.1607730113/-/DCSupplemental.

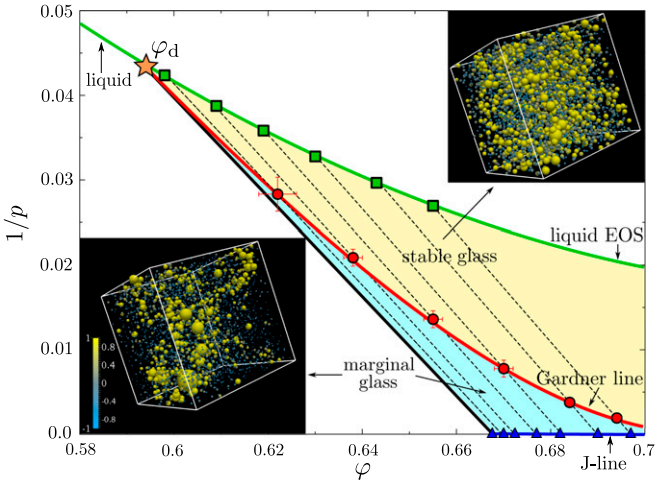

Fig. 1. Two glass phases. Inverse reduced pressure–packing fraction ($1/p$ v φ) phase diagram for polydisperse hard spheres. The equilibrium simulation results at φ_g (green squares) are fitted to the liquid EOS (Eq. **1**, green line). The dynamical cross-over, φ_d, is obtained from the liquid dynamics. Compression annealing from φ_g up to jamming (blue triangles) follows a glass EOS (fit to Eq. **3**, dashed lines). At φ_G (red circles and line) with a finite p, stable glass states transform into marginally stable glasses. Snapshots illustrate spatial heterogeneity above and below φ_G, with sphere diameters proportional to the linear cage size and colors encoding the relative cage size, u_i (see the text).

obtaining the liquid equation of state (EOS). The liquid EOS for the reduced pressure $p=\beta P/\rho$, where ρ is the number density, β is the inverse temperature, and P is the system pressure, is described by

$$p_{\text{liquid}}(\varphi)=1+f(\varphi)[p_{\text{CS}}(\varphi)-1], \qquad [1]$$

with $p_{\text{CS}}(\varphi)$ from ref. 13

$$p_{\text{CS}}(\varphi)=\frac{1}{1-\varphi}+\frac{3s_1s_2}{s_3}\frac{\varphi}{(1-\varphi)^2}+\frac{s_2^3}{s_3^2}\frac{(3-\varphi)\varphi^2}{(1-\varphi)^3}, \qquad [2]$$

where s_k is the kth moment of $P_\sigma(\sigma)$, and $f(\varphi)=0.005-\tanh[14(\varphi-0.79)]$ are fitted quantities. The structure of the equilibrium configurations generated by the swap algorithm has been carefully analyzed. Unlike for other glass formers (14, 15), no signs of orientational or crystalline order were observed (16, 17). Following the strategy of ref. 18, we also obtain the mode-coupling theory dynamical cross-over $\varphi_d=0.594(1)$ (*SI Appendix*). We have not analyzed the compression of equilibrium configurations with $\varphi_g<\varphi_d$, as done in earlier studies (19, 20), because structural relaxation is not well decoupled from vibrational dynamics, although the obtained jammed states should have equivalent properties.

Second, we use these liquid configurations as starting points for standard molecular dynamics simulations during which the system is compressed out of equilibrium up to various target $\varphi>\varphi_g$ (21). Annealing is achieved by growing spheres following the Lubachevsky–Stillinger algorithm (21) at a constant growth rate $\gamma_g=10^{-3}$ (see *SI Appendix* for a discussion on the γ_g -dependence). The average particle diameter, $\overline{\sigma}$, serves as unit length, and the simulation time is expressed in units of $\sqrt{\beta m\overline{\sigma}^2}$. To obtain thermal and disorder averaging, this procedure is repeated over N_s samples ($N_s\approx 150$ for $N=1{,}000$ and $N_s=50$ for $N=8{,}000$), each with different initial equilibrium configurations at φ_g, and over $N_{\text{th}}=64-19{,}440$ independent thermal (quench) histories for each sample. Quantities reported here are averaged over $N_s\times N_{\text{th}}$ quench histories, unless otherwise specified. The nonequilibrium glass EOSs associated with this compression (dashed lines) terminate (at infinite pressure) at inherent structures that correspond, for hard spheres, to jammed configurations (blue triangles). To capture the glass EOSs, we use a free-volume scaling around the corresponding jamming point φ_J

$$p_{\text{glass}}(\varphi;\varphi_g)=\frac{C}{\varphi_J(\varphi_g)-\varphi}, \qquad [3]$$

where the constant C weakly depends on φ_g.

Our numerical protocol is analogous to varying the cooling rate—and thus the glass transition temperature—of thermal glasses, and then further annealing the resulting amorphous solid. Each value of φ_g indeed selects a different glass, ranging from the onset of sluggish liquid dynamics around the dynamical cross-over (1, 2), φ_d, to the very dense liquid regime where diffusion and vibrations (β-relaxation processes) are fully separated (2). For sufficiently large φ_g, we thus obtain unimpeded access to the only remaining glass dynamics, i.e., β-relaxation processes (4).

Growing Timescales

A central observable to characterize glass dynamics is the mean-squared displacement (MSD) of particles from position $\boldsymbol{r}_i(t_w)$

$$\Delta(t,t_w)=\frac{1}{N}\sum_{i=1}^{N}\left\langle|\boldsymbol{r}_i(t+t_w)-\boldsymbol{r}_i(t_w)|^2\right\rangle, \qquad [4]$$

averaged over both thermal fluctuations and disorder, where time t starts after waiting time t_w when compression has reached the target φ. The MSD plateau height at long times quantifies the average cage size (*SI Appendix*). Because some of the smaller particles manage to leave their cages, the sum in Eq. **4** is here restricted to the larger half of the particle size distribution (*SI Appendix*). When φ is not too large, $\varphi\gtrsim\varphi_g$, the plateau emerges quickly, as suggested by the traditional view of caging in glasses (Fig. 2*A*).

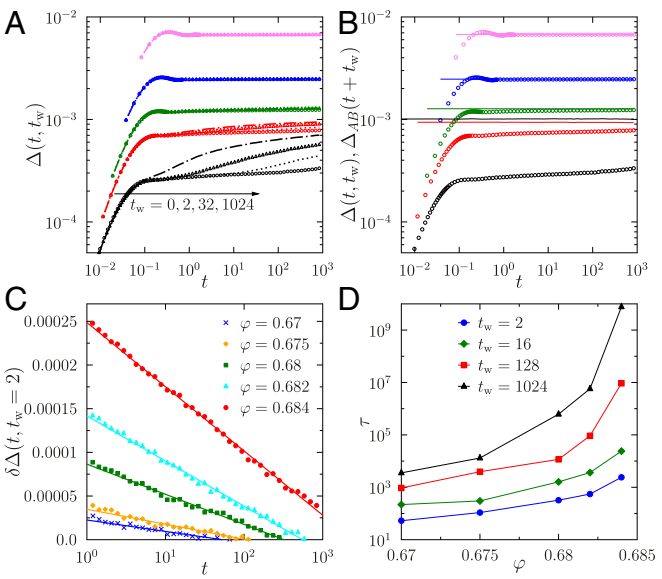

Fig. 2. Emergence of slow vibrational dynamics. (*A*) Time evolution of $\Delta(t,t_w)$ for several t_w and φ (from top to bottom, $\varphi=0.645, 0.67, 0.68, 0.684, 0.688$), following compression from $\varphi_g=0.643$. For $\varphi\gtrsim\varphi_G=0.684$, $\Delta(t,t_w)$ displays strong aging. (*B*) Comparison between $\Delta(t,t_w)$ (points) and $\Delta_{AB}(t+t_w)$ (lines) for the longest waiting time $t_w=1{,}024$. For $\varphi<\varphi_G$ both observables converge to the same value within the time window considered, but not for $\varphi>\varphi_G$. (*C*) The time evolution of $\delta\Delta(t,t_w)$ at $t_w=2$ displays a logarithmic tail, which provides a characteristic relaxation time τ. (*D*) As φ approaches φ_G, τ grows rapidly for any t_w.

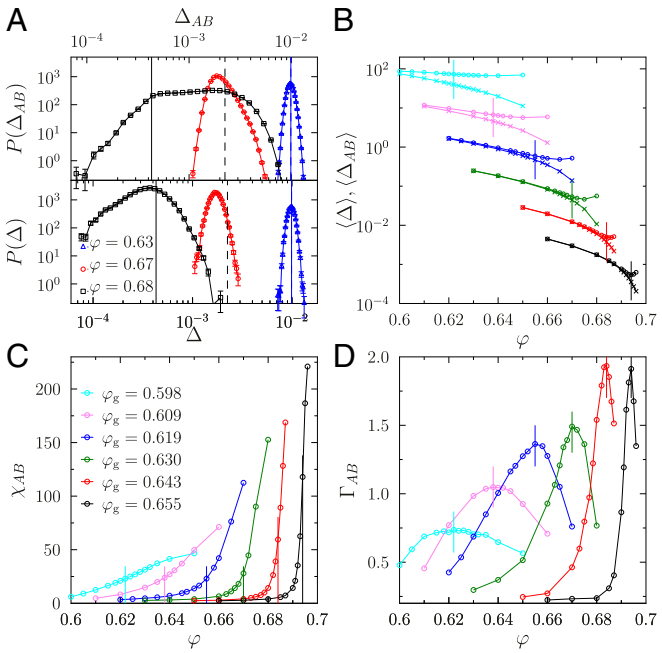

Fig. 3. Global fluctuations of the order parameter. (*A*) Probability distribution functions for Δ_{AB} and Δ above, at, and below the Gardner cross-over, $\varphi_G = 0.670(2)$ for $\varphi_g = 0.630$. Vertical lines mark $\langle\Delta\rangle$ (solid) and $\langle\Delta_{AB}\rangle$ (dashed), which also represent the peak positions. (*B*) Comparing $\langle\Delta\rangle$ and $\langle\Delta_{AB}\rangle$ shows that the average values separate for $\varphi \gtrsim \varphi_G$ (Data are multiplied by 5^k, where $k = 0,1,\ldots,5$ for $\varphi = 0.655, 0.643, \ldots, 0.598$, respectively.) Around φ_G, (*C*) the global susceptibility χ_{AB} grows very rapidly, and (*D*) the skewness Γ_{AB} peaks. Numerical estimates for φ_G are indicated by vertical segments.

When the glass is compressed beyond a certain φ_G, however, $\Delta(t, t_w)$ displays both a strong dependence on the waiting time t_w, i.e., aging, and a slow dynamics, as captured by the emergence of two plateaus. These effects suggest a complex vibrational dynamics. Aging, in particular, provides a striking signature of a growing timescale associated with vibrations, revealing the existence of a "glass transition" deep within the glass phase.

To determine the timescale associated with this slowdown, we estimate the distance between independent pairs of configurations by first compressing two independent copies, A and B, from the same initial state at φ_g to the target φ, and then measuring their relative distance

$$\Delta_{AB}(t) = \frac{1}{N}\sum_{i=1}^{N}\left\langle \left|\boldsymbol{r}_i^A(t) - \boldsymbol{r}_i^B(t)\right|^2 \right\rangle, \qquad [5]$$

so that $\Delta_{AB}(t \to \infty) \simeq \Delta(t \to \infty, t_w \to \infty)$, as shown in Fig. 2*B*. The two copies share the same positions of particles at φ_g, but are assigned different initial velocities drawn from the Maxwell–Boltzmann distribution. The time evolution of the difference $\delta\Delta(t, t_w) = \Delta_{AB}(t_w + t) - \Delta(t, t_w)$ indicates that whereas the amplitude of particle motion naturally becomes smaller as φ increases, the corresponding dynamics becomes slower (Fig. 2*C*). In other words, as φ grows particles take longer to explore a smaller region of space. In a crystal, by contrast, $\delta\Delta(t, t_w)$ decays faster under similar circumstances. A relaxation timescale, τ, can be extracted from the decay of $\delta\Delta(t, t_w)$ at large t, whose logarithmic form, $\delta\Delta(t, t_w) \sim 1 - \ln t/\ln\tau$, is characteristic of the glassiness of vibrations. As $\varphi \to \varphi_G$, we find that τ dramatically increases (Fig. 2*D*), which provides direct evidence of a marked cross-over characterizing the evolution of the glass upon compression.

Global Fluctuations of the Order Parameter

This sharp dynamical cross-over corresponds to a loss of ergodicity inside the glass, i.e., time and ensemble averages yield different results. To better characterize this cross-over, we define a timescale τ_{cage} for the onset of caging [$\tau_{cage} \approx \mathcal{O}(1)$; *SI Appendix*], and the corresponding order parameters $\Delta_{AB} \equiv \Delta_{AB}(\tau_{cage})$ and $\Delta \equiv \Delta(\tau_{cage}, t_w = 0)$.

The evolution of the probability distribution functions, $P(\Delta_{AB})$ and $P(\Delta)$, as well as their first moments, $\langle\Delta_{AB}\rangle$ and $\langle\Delta\rangle$, are presented in Fig. 3 *A* and *B* for a range of densities across φ_G. For $\varphi < \varphi_G$, dynamics is fast, $\langle\Delta_{AB}\rangle$ and $\langle\Delta\rangle$ coincide, and $P(\Delta_{AB})$ and $P(\Delta)$ are narrow and Gaussian-like. For $\varphi > \varphi_G$, however, the MSD does not converge to its long-time limit, $\langle\Delta\rangle < \langle\Delta_{AB}\rangle$, which indicates that configuration space explored by vibrational motion is now broken into mutually inaccessible regions. Interestingly, the slight increase of $\langle\Delta_{AB}\rangle$ with φ in this regime (Fig. 3*B*) suggests that states are then pushed further apart in phase space, which is consistent with theoretical predictions (11). When compressing a system across φ_G, its dynamics explores only a restricted part of phase space. As a result, Δ_{AB} displays pronounced, non-Gaussian fluctuations (Fig. 3*A*). Repeated compressions from a same initial state at φ_g may end up in distinct states, which explains why Δ_{AB} is typically much larger and more broadly fluctuating than Δ (Fig. 3*A*). These results are essentially consistent with theoretical predictions (9, 11), which suggest that for $\varphi > \varphi_G$, $P(\Delta_{AB})$ should separate into two peaks connected by a wide continuous band with the left-hand peak continuing the single peak of $P(\Delta)$. The very broad distribution of Δ_{AB} further suggests that spatial correlations develop as $\varphi \to \varphi_G$, yielding strongly correlated states at larger densities.

To quantify these fluctuations we measure the variance χ_{AB} and skewness Γ_{AB} (*SI Appendix* and ref. 11) of $P(\Delta_{AB})$ (Fig. 3 *C* and *D*). The global susceptibility χ_{AB} is very small for $\varphi < \varphi_G$ and grows rapidly as φ_G is approached, increasing by about two decades for the largest φ_g considered (Fig. 3*C*). Whereas χ_{AB} quantifies the increasing width of the distributions, Γ_{AB} reveals a change in their shapes. For each φ_g we find that Γ_{AB} is small on both sides of φ_G with a pronounced maximum at $\varphi = \varphi_G$ (Fig. 3*D*). This reflects the roughly symmetric shape of $P(\Delta_{AB})$ around $\langle\Delta_{AB}\rangle$ on both sides of φ_G and the development of an asymmetric tail for large Δ_{AB} around the cross-over, a known signature of sample-to-sample fluctuations in spin glasses (22) and mean-field glass models (11). Note that because the skewness maximum gives the clearest numerical estimate of φ_G, we use it to determine the values reported in Fig. 1.

Growing Correlation Length

The rapid growth of χ_{AB} in the vicinity of φ_G suggests the concomitant growth of a spatial correlation length, ξ. Its measurement

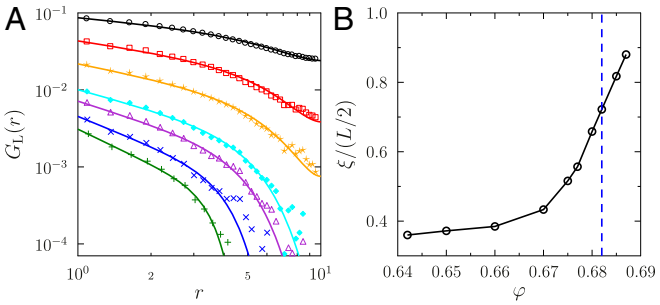

Fig. 4. Growing correlation length. (*A*) Spatial correlator $G_L(r)$ (Eq. **6**) for different φ (from bottom to top, $\varphi = 0.65, 0.67, 0.675, 0.677, 0.68, 0.682, 0.687$) annealed from $\varphi_g = 0.640$, with $N = 8{,}000$ (larger systems are used here to significantly measure the growth of ξ). (*B*) Fitting $G_L(r)$ to Eq. **7** (lines in *A*) provides the correlation length ξ, which grows with φ and becomes comparable to the linear system size upon approaching $\varphi_G = 0.682(2)$ (dashed line).

requires spatial resolution of the fluctuations of Δ_{AB}, hence for each particle i we define $u_i = (|\boldsymbol{r}_i^A - \boldsymbol{r}_i^B|^2/\langle\Delta_{AB}\rangle) - 1$ to capture its contribution to deviations around the average $\langle\Delta_{AB}\rangle$. A first glimpse of these spatial fluctuations is offered by snapshots of the u_i field (Fig. 1), which appear featureless for $\varphi < \varphi_G$, but highly structured and spatially correlated for $\varphi \gtrsim \varphi_G$. More quantitatively, we define the spatial correlator

$$G_L(r) = \frac{\left\langle \sum_{\mu=1}^{3} \sum_{i\neq j} u_i u_j \delta\left(r - \left|\boldsymbol{r}_{i,\mu}^A - \boldsymbol{r}_{j,\mu}^A\right|\right)\right\rangle}{\left\langle \sum_{\mu=1}^{3} \sum_{i\neq j} \delta\left(r - \left|\boldsymbol{r}_{i,\mu}^A - \boldsymbol{r}_{j,\mu}^A\right|\right)\right\rangle}, \quad [6]$$

where $\boldsymbol{r}_{i,\mu}$ is the projection of the particle position along direction μ. Even for the larger system size considered, measuring $G_L(r)$ is challenging because spatial correlations quickly become long-ranged as $\varphi \to \varphi_G$ (Fig. 4*A*). Fitting the results to an empirical form that takes into account the periodic boundary conditions in a system of linear size L,

$$G_L(r) \sim \frac{1}{r^a} e^{-(r/\xi)^b} + \frac{1}{(L-r)^a} e^{-[(L-r)/\xi]^b}, \quad [7]$$

where a and b are fitting parameters, nonetheless confirms that ξ grows rapidly with φ and becomes of the order of the simulation box at $\varphi > \varphi_G$ (Fig. 4*B*). Note that although probed using a dynamical observable, the spatial correlations captured by $G_L(r)$ are conceptually distinct from the dynamical heterogeneity observed in supercooled liquids (23), which is transient and disappears once the diffusive regime is reached.

Experimental Consequences

The system analyzed in this work is a canonical model for colloidal suspensions and granular media. Hence, experiments along the lines presented here could be performed to investigate more closely vibrational dynamics in colloidal and granular glasses, using a series of compressions to extract Δ and Δ_{AB}. Experiments are also possible in molecular and polymeric glasses, for which the natural control parameter is temperature T instead of density. Let us therefore rephrase our findings from this viewpoint. As the system is cooled, the supercooled liquid dynamics is arrested at the laboratory glass transition temperature T_g. As the resulting glass is further cooled its phase space transforms, around a well-defined Gardner temperature $T_G < T_g$, from a simple state (akin to that of a crystal) into a more complex phase composed of a large number of glassy states (see *SI Appendix* for a discussion of the phase diagram as a function of T).

Around T_G, vibrational dynamics becomes increasingly heterogeneous (Fig. 1), slow (Fig. 2), fluctuating from realization to realization (Fig. 3), and spatially correlated (Fig. 4). The β-relaxation dynamics inside the glass thus becomes highly cooperative (24, 25) and ages (26). The fragmentation of phase space below T_G also gives rise to a complex response to mechanical perturbations in the form of plastic irreversible events, in which the system jumps from one configuration to another (4, 6, 27). This expectation stems from the theoretical prediction that the complex phase at $T < T_G$ is marginally stable (9), which implies that glass states are connected by very low energy barriers, resulting in strong responses to weak perturbations (7).

A key prediction is that the aforementioned anomalies appear simultaneously around a T_G that is strongly dependent on the scale T_g selected by the glass preparation protocol. Annealed glasses with lower T_g are expected to present a sharper Gardner-like cross-over, at an increasingly lower temperature. Numerically, we produced a substantial variation of φ_g by using an efficient Monte Carlo algorithm to bypass the need for a broad range of compression rates. In experiments a similar or even larger range of T_g can be explored (28), using poorly annealed glasses from hyperquenching (29) and ultrastable glasses from vapor deposition (30–32). We expect ultrastable glasses, in particular, to display strongly enhanced glass anomalies, consistent with recent experimental reports (33–35). Interestingly, a Gardner-like regime may also underlie the anomalous aging recently observed in individual proteins (36).

Conclusion

Since its prediction in the mean-field limit, the Gardner transition has been regarded as a key ingredient to understand the physical properties of amorphous solids. Understanding the role of finite-dimensional fluctuations is a difficult theoretical problem (37). Our work shows that clear signs of an apparent critical behavior can be observed in three dimensions, at least in a finite-size system, which shows that the correlation length becomes at least comparable to the system size as φ approaches φ_G. Although the fate of these findings in the thermodynamic limit remains an open question, the remarkably large signature of the effect strongly suggests that the Gardner phase transition paradigm is a promising theoretical framework for a universal understanding of the anomalies of solid amorphous materials, from granular materials to glasses, foams, and proteins.

ACKNOWLEDGMENTS. P.C. acknowledges support from the Alfred P. Sloan Foundation and National Science Foundation (NSF DMR-1055586). B.S. acknowledges the support by Ministerio de Economía y Competitividad (MINECO) (Spain) through Research Contract FIS2012-35719-C02. This project has received funding from the European Union's Horizon 2020 Research and Innovation Programme under the Marie Skłodowska-Curie Grant Agreement 654971, as well as from the European Research Council (ERC) under the European Union's Seventh Framework Programme (FP7/2007-2013)/ERC Grant Agreement 306845. This work was granted access to the High-Performance Computing (HPC) resources of Mésocentre de Calcul-Université de Recherche Paris Sciences et Lettres (MesoPSL) financed by the Region Ile de France and the project Equip@Meso (Reference ANR-10-EQPX-29-01) of the program Investissements d'Avenir supervised by the Agence Nationale pour la Recherche. This project has received funding from the ERC under the European Union's Horizon 2020 Research and Innovation Programme (Grant Agreement 694925).

1. Berthier L, Biroli G (2011) Theoretical perspective on the glass transition and amorphous materials. *Rev Mod Phys* 83(2):587–645.
2. Cavagna A (2009) Supercooled liquids for pedestrians. *Phys Rep* 476(4):51–124.
3. Phillips WA (1987) Two-level states in glasses. *Rep Prog Phys* 50(12):1657.
4. Goldstein M (2010) Communications: Comparison of activation barriers for the Johari-Goldstein and alpha relaxations and its implications. *J Chem Phys* 132(4):041104.
5. Malinovsky VK, Sokolov AP (1986) The nature of boson peak in Raman scattering in glasses. *Solid State Commun* 57(9):757–761.
6. Hentschel HGE, Karmakar S, Lerner E, Procaccia I (2011) Do athermal amorphous solids exist? *Phys Rev E Stat Nonlin Soft Matter Phys* 83(6 Pt 1):061101.
7. Müller M, Wyart M (2015) Marginal stability in structural, spin, and electron glasses. *Annu Rev Condens Matter Phys* 6:177–200.
8. Wolynes P, Lubchenko V, eds (2012) *Structural Glasses and Supercooled Liquids: Theory, Experiment, and Applications* (Wiley, Hoboken, NJ).
9. Charbonneau P, Kurchan J, Parisi G, Urbani P, Zamponi F (2014) Fractal free energy landscapes in structural glasses. *Nat Commun* 5:3725.
10. Gardner E (1985) Spin glasses with *p*-spin interactions. *Nucl Phys B* 257:747–765.
11. Charbonneau P, et al. (2015) Numerical detection of the Gardner transition in a mean-field glass former. *Phys Rev E Stat Nonlin Soft Matter Phys* 92(1):012316.
12. Grigera TS, Parisi G (2001) Fast Monte Carlo algorithm for supercooled soft spheres. *Phys Rev E Stat Nonlin Soft Matter Phys* 63(4 Pt 2):045102.
13. Boublik T (1970) Hard sphere equation of state. *J Chem Phys* 53(1):471.
14. Russo J, Tanaka H (2015) Assessing the role of static length scales behind glassy dynamics in polydisperse hard disks. *Proc Natl Acad Sci USA* 112(22):6920–6924.
15. Flenner E, Szamel G (2015) Fundamental differences between glassy dynamics in two and three dimensions. *Nat Commun* 6:7392.
16. Berthier L, Coslovich D, Ninarello A, Ozawa M (2016) Equilibrium sampling of hard spheres up to the jamming density and beyond. *Phys Rev Lett* 116(23):238002.
17. Yaida S, Berthier L, Charbonneau P, Tarjus G (2015) Point-to-set lengths, local structure, and glassiness. arXiv:1511.03573.
18. Charbonneau P, Jin Y, Parisi G, Zamponi F (2014) Hopping and the Stokes-Einstein relation breakdown in simple glass formers. *Proc Natl Acad Sci USA* 111(42):15025–15030.
19. Chaudhuri P, Berthier L, Sastry S (2010) Jamming transitions in amorphous packings of frictionless spheres occur over a continuous range of volume fractions. *Phys Rev Lett* 104(16):165701.
20. Ozawa M, Kuroiwa T, Ikeda A, Miyazaki K (2012) Jamming transition and inherent structures of hard spheres and disks. *Phys Rev Lett* 109(20):205701.
21. Skoge M, Donev A, Stillinger FH, Torquato S (2006) Packing hyperspheres in high-dimensional Euclidean spaces. *Phys Rev E Stat Nonlin Soft Matter Phys* 74(4 Pt 1): 041127.
22. Parisi G, Rizzo T (2013) Critical dynamics in glassy systems. *Phys Rev E Stat Nonlin Soft Matter Phys* 87(1):012101.
23. Berthier L, Biroli G, Bouchaud JP, Cipelletti L, van Saarloos W, eds (2011) *Dynamical Heterogeneities and Glasses* (Oxford Univ Press, Oxford).
24. Cohen Y, Karmakar S, Procaccia I, Samwer K (2012) The nature of the β-peak in the loss modulus of amorphous solids. *Europhys Lett* 100(3):36003.
25. Bock D, et al. (2013) On the cooperative nature of the β-process in neat and binary glasses: A dielectric and nuclear magnetic resonance spectroscopy study. *J Chem Phys* 139(6):064508.

26. Leheny RL, Nagel SR (1998) Frequency-domain study of physical aging in a simple liquid. *Phys Rev B* 57(9):5154.
27. Brito C, Wyart M (2009) Geometric interpretation of previtrification in hard sphere liquids. *J Chem Phys* 131(2):024504.
28. Rössler E, Sokolov AP, Kisliuk A, Quitmann D (1994) Low-frequency Raman scattering on different types of glass formers used to test predictions of mode-coupling theory. *Phys Rev B Condens Matter* 49(21):14967–14978.
29. Velikov V, Borick S, Angell CA (2001) The glass transition of water, based on hyperquenching experiments. *Science* 294(5550):2335–2338.
30. Swallen SF, et al. (2007) Organic glasses with exceptional thermodynamic and kinetic stability. *Science* 315(5810):353–356.
31. Singh S, Ediger MD, de Pablo JJ (2013) Ultrastable glasses from in silico vapour deposition. *Nat Mater* 12(2):139–144.
32. Hocky GM, Berthier L, Reichman DR (2014) Equilibrium ultrastable glasses produced by random pinning. *J Chem Phys* 141(22):224503.
33. Pérez-Castañeda T, Rodríguez-Tinoco C, Rodríguez-Viejo J, Ramos MA (2014) Suppression of tunneling two-level systems in ultrastable glasses of indomethacin. *Proc Natl Acad Sci USA* 111(31):11275–11280.
34. Liu X, Queen DR, Metcalf TH, Karel JE, Hellman F (2014) Hydrogen-free amorphous silicon with no tunneling states. *Phys Rev Lett* 113(2):025503.
35. Yu HB, Tylinski M, Guiseppi-Elie A, Ediger MD, Richert R (2015) Suppression of β relaxation in vapor-deposited ultrastable glasses. *Phys Rev Lett* 115(18):185501.
36. Hu X, et al. (2015) The dynamics of single protein molecules is non-equilibrium and self-similar over thirteen decades in time. *Nat Phys* 12:171–174.
37. Urbani P, Biroli G (2015) Gardner transition in finite dimensions. *Phys Rev B* 91(10): 100202.